Additional sub-gap conductance enhancement in nanoscale Andreev point contact junctions

2007 J. Phys.: Condens. Matter 19 136211

(http://iopscience.iop.org/0953-8984/19/13/136211)

IOP PUBLISHING JOURNAL OF PHYSICS: CONDENSED MATTER

J. Phys.: Condens. Matter **19** (2007) 136211 (8pp) doi:10.1088/0953-8984/19/13/136211

Additional sub-gap conductance enhancement in nanoscale Andreev point contact junctions

A T Hindmarch, C H Marrows and B J Hickey

School of Physics and Astronomy, EC Stoner Laboratory, University of Leeds, Leeds, LS2 9JT, UK

E-mail: a.t.hindmarch@leeds.ac.uk

Received 22 November 2006, in final form 14 February 2007
Published 13 March 2007
Online at stacks.iop.org/JPhysCM/19/136211

Abstract

We demonstrate an enhancement in the sub-gap conductance in Nb/Al/Cu nanoscale pinhole junctions, significantly larger than the conductance doubling expected from the point contact Andreev reflection process. Such an enhancement is not observed in standard micrometre-driven NbTi/Cu wire-tipped junctions where the expected sub-gap conductance is regained. This additional sub-gap conductance arises due to regions of the pinhole junction being driven into the normal state due to current-induced pair breaking, causing the Andreev reflection process to occur at different interfaces within the contact structure as the bias is increased. This work demonstrates, again, that a great deal of care must be taken in interpreting Andreev reflection measurements in nanoscale junctions, in particular with regard to extracting accurate spin polarization.

(Some figures in this article are in colour only in the electronic version)

1. Introduction

The enhanced electrical conductance across a normal metal/superconductor (N/SC) interface at sub-gap bias was, over 40 years ago, explained as being due to the process of retro-reflection of electrons incident on the N/SC boundary as holes—and the subsequent formation of a Cooper pair which continues in the forward direction [1]; the process later being eponymously named 'Andreev reflection' (AR). This effect results in a double contribution to the conductance since two electrons—a Cooper pair—continue into the superconductor for each electron which is Andreev reflected.

An appealing consequence for modern spintronics is that, for the case of a ferromagnetic metal (FM) where the conduction electron spin-populations are unequal, the sub-gap conductance enhancement due to the AR process is somewhat suppressed in direct relation to the spin polarization; the probability for electrons to pair with others of opposite spin is reduced.

Use of the point contact Andreev reflection (PCAR) [2, 3] technique has been extensively reported, particularly in the quest to develop and demonstrate half-metallic magnetic materials for spintronics applications. For a junction with ideal transmission, the spin polarization can be simply obtained from the zero-bias conductance from

$$\frac{1}{G_{\mathrm{N}}}\frac{\partial I}{\partial V}\bigg|_{V=0} = 2(1-P)$$

where G_{N} is the normal-state conductance and P the spin polarization [2]. A suitable theoretical description of the sub-gap conductance enhancement due to the AR process in point contacts, based on the one-dimensional Bogoliubov–de Gennes formalism, has been provided by Blonder *et al* [4], commonly referred to as the BTK model. Several models have been proposed to determine spin-polarization in cases other than the ideal limit; that which is usually obtained in experiments due to band-structure mismatch, dirty interfaces etc; based on a 'modified-BTK' approach [5, 6] and compared to first principles calculation [7]. The search for an entirely unambiguous half-metallic PCAR signature is ongoing.

There is presently renewed interest in sub-micron and nanoscale patterned junctions [3, 8, 9], which are now particularly relevant in order to ensure that the Sharvin limit [10] for one-dimensional transport across the interface—the lateral contact dimension must be small in comparison to the mean-free-path—is met for highly resistive materials, as in the case of many candidate half-metals at low temperatures.

In recent years, the accuracy of the values of spin polarization obtained using this technique have been brought into question, due to the complex physics that the models must capture. It has been suggested both that the commonly applied modified-BTK approach is insufficient to model a FM/SC interface [7, 8], and that stray magnetic fields may affect the measured dependence of spin polarization on N/SC interface transparency [11]. We demonstrate an additional potential pitfall in interpreting such AR data, due to critical current density effects in nanoscale junctions modifying the apparent sub-gap conductance compared to that due solely to the AR process.

2. Experimental details

The N/SC junctions discussed in this work comprise two distinct types. Those of the first type, standard micrometre contact junctions, comprise a superconducting wire tip, in this case an NbTi filamentary wire etched in aqua-regia to leave a single bare filament, which is brought into contact with a metal film or foil using a micrometre screw-gauge. This type of junction has been reported extensively elsewhere [2, 5, 11]. A schematic of this measurement arrangement is shown in the inset to figure 1. For this type of junction, with a conventional metal film, we typically obtain junction resistances in the range of 1–25 Ω at 4.2 K, consistent with those obtained in other studies reported in the literature [5].

The second type of junction, nanoscale pinhole junctions, are formed by deliberately creating a pinhole via electromigration in an insulating AlO_x layer separating superconducting and normal metal layers. These junctions are deposited by magnetron sputtering and have a crossed electrode structure, similar to those used in [12] where pinholes were formed as part of a non-optimal deposition process rather than being deliberately created afterwards. The junctions are deposited on to pieces cut from a Si(001) wafer, and have a layer sequence of Nb[900 Å]/AlO_x[∼ 30 Å]/Cu[500 Å], with a schematic of the junction structure being shown in the inset to figure 2. A *continuous* AlO_x barrier is formed by exposing the deposited Al film to an oxygen plasma *in situ* for 300 s [13]. These AlO_x tunnel junctions have an active area of 500 × 500 μm^2 and have a resistance of ∼800–1200 Ω at 10 K. The junctions display

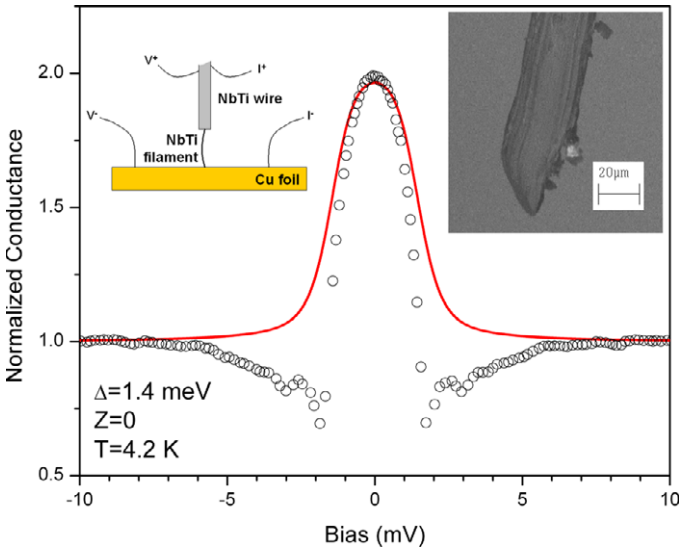

Figure 1. Micrometre-driven PCAR measurement of a NbTi filament pressed onto a Cu foil at 4.2 K. The normal-state contact resistance is ∼1 Ω. Note the doubling of conductance within the gap region. The fit shown is to the standard BTK model [4] where the parameter Δ is the SC energy gap. The BTK 'barrier strength' Z and temperature T are fixed, and the insets show (left) a schematic of the measurement arrangement and (right) an SEM image of a NbTi filament tip after etching.

I–V characteristics consistent with tunnelling behaviour at all temperatures, indicating the continuity of the oxide barrier [12]. The relatively low junction resistance suggests that the Al film is not completely oxidized; the oxidation process for Al is typically self-limiting to ∼20 Å [14], so there is still a thin metallic aluminium layer separating the Nb lower electrode and AlO_x tunnel barrier. The surface roughness of the niobium lower electrode produces local fluctuations in the barrier thickness, resulting in tunnelling 'hot-spots' which are the most likely places for the pinhole to nucleate.

The pinhole junction is formed by slowly ramping the applied voltage bias until dielectric breakdown occurs at a bias of around 2.0–2.1 V. Once breakdown occurs, the resistance of the junction immediately falls to around 1–10 Ω and the corresponding voltage drop across the junction relative to the leads falls to significantly below the dielectric breakdown threshold. Such abrupt breakdown indicates that the pinhole is created by an 'intrinsic' breakdown mechanism, due to the electric field driven dielectric breakdown of a well-formed oxide [15]. When the Nb layer is cooled through its transition temperature, the unoxidized Al film *and* Al pinhole are driven superconducting by the proximity effect[1]. The alternative breakdown mechanism, 'extrinsic' breakdown, occurs when a pre-existing structural pinhole is enlarged due to Joule heating. In this case the initial I–V characteristic would already show Andreev reflection due to the pinhole [12] and the junction breakdown would not occur abruptly [15].

Conductance and derivative (second harmonic) measurements are made by standard four-point modulation techniques using dual trigger-linked lock-in amplifiers. Micrometre contact junction measurements are made at 4.2 K in a ^{4}He immersion cryostat, and pinhole junction measurements at 2 K in a standard ^{4}He cryostat.

[1] Junctions with FM top electrodes show a suppressed Andreev reflection probability, indicating that the Al pinhole is driven into a SC state.

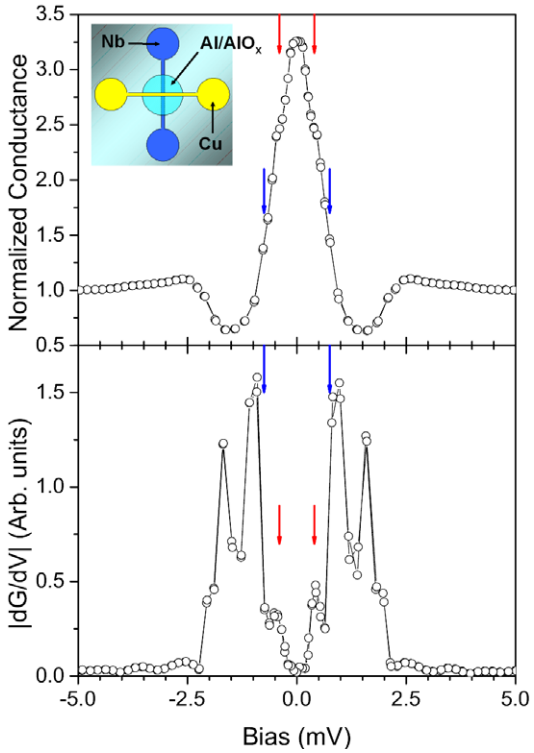

Figure 2. PCAR conductance measurement (upper) for a Nb/Al/Cu pinhole junction at 2 K and (lower) measured second-harmonic spectrum, which highlights points of inflection in the conductance data. Short (red) arrows indicate a change in conductance at low bias (0.4 mV) due to the onset of the normal state in the Al pinhole, whilst long (blue) arrows indicate a similar change (at 0.75 mV) due to the onset of the normal state in the Al film layer. The inset shows a schematic plan-view of the crossed-electrode junction structure. The pinhole contact through the AlO_x insulating barrier is within the region of electrode intersection.

3. Results

Figure 1 shows the PCAR spectrum for a micrometre-driven contact junction onto a Cu foil. We observe the expected factor of 2 enhancement in the sub-gap conductance, and the data is reasonably described by the BTK model with a sensible value for the Δ parameter. The dip features observed just above the gap energy are commonly observed in other PCAR measurements [2, 5, 12], although they are not, as yet, satisfactorily understood. The inset shows a scanning electron micrograph of a typical etched NbTi tip, demonstrating the mechanical contact diameter to be $\sim$30 μm, placing an upper bound on the *effective electrical* contact diameter. In the upper frame of figure 2 we show the corresponding PCAR spectrum for a Nb/Al/Cu pinhole junction. The normal-state resistance of this junction at 10 K is 4.5 Ω; it is possible to estimate the area A of the contact from its normal-state conductance as

$$G_{\mathrm{N}} \sim \frac{e^2}{\hbar} k_{\mathrm{F}}^2 A$$

where $k_{\mathrm{F}} = 1.75$ Å^{-1} is the free-electron Fermi wavevector in aluminium. Thus for a junction resistance of 4.5 Ω and assuming conduction through a single pinhole, we can estimate an upper limit on the pinhole effective electrical contact diameter of roughly 50 nm, and anticipate

a slightly larger effective diameter for the NbTi/Cu contact junction, around 0.1–0.2 μm. Surprisingly, the sub-gap conductance in this nanoscale pinhole junction is enhanced by a factor of 3.25; significantly greater than the factor of 2 due to a simple AR mechanism and, of course, impossible to model within the standard BTK framework.

A clue to the origin of this anomalous conductance enhancement may be gained from observing closely the features in the PCAR spectrum. In addition to the dips at just above the gap energy—suggested as perhaps being related to a proximity effect [5]—there are several inflections within the sub-gap peak structure itself. This may be more clearly seen from the measured derivative spectrum, shown in the lower frame of figure 2; such derivative measurements are commonly used to accentuate features in conductance data [14]. In addition to features relating to the conductance dips, the derivative spectrum shows peaks at $|V| \sim 0.4$ and $\sim$0.75 mV, corresponding to inflections within the sub-gap peak. These sub-gap features are indicated by short (red), and longer (blue) arrows in figure 2. We note that one of these features is suggestively close to the SC gap energy of aluminium, $\Delta(0)_{\mathrm{Al}} = 0.34$ meV, possibly indicating that these inflections are due to different regions of the pinhole contact being driven from the SC state as the junction bias increases. This first feature occurs at a junction bias of $\sim$0.4 mV where the conductance G is 0.57 S. For a 50 nm diameter contact this results in a current density of $J \sim 100$ GA m^{-2}, in reasonable agreement with the zero-temperature pair breaking critical current density $J_{\mathrm{C}}(0)$ obtained from sub-micron aluminium strips [16].

An alternative explanation for the reduced conductance at higher bias may be Joule heating of the sample. For the pinhole junction in figure 2 the Joule heating power dissipated at high bias is roughly 10 μW; insufficient to cause any significant heating of the sample. No significant temperature change was recorded over the duration of the measurements. At a temperature of 2 K the resistivity of the copper electrode film, or of the aluminium pinhole or film is, to a good approximation, independent of temperature. It was suggested by Upadhyay *et al* [3] that high current densities in their sub-10 nm diameter Pb/Co contacts could be the reason for the discrepancies between their data and fits to their proposed three-dimensional modified-BTK model, lending further credence to the idea that we are driving the aluminium pinhole into the normal state. Possible critical current effects have also been discussed by Sheet *et al* [17].

Assuming the inflection at 0.4 mV to be caused by the current density in the Al pinhole exceeding its critical current density J_{C} and thus driving the pinhole normal, we can suppose that for bias below 0.4 mV, AR occurs at the SC aluminium (pinhole)/N copper interface, whereas above this bias it now occurs at a SC aluminium (film)/N aluminium (pinhole) interface as depicted in the inset to figure 3. As neither Cu nor Al are spin polarized, either of these AR processes would result in a factor of 2 enhancement in conductance over the normal-state conductance *of that particular interface*. We point out that the conductance enhancement for junctions with lower Δ may appear to be reduced due to thermal broadening. In the zero temperature limit the conductance doubling for a particular interface is present up to the energy gap edge for that interface. At higher bias, 0.75 mV, another feature occurs in the PCAR spectrum—which would seem likely to be due to the SC aluminium film (in the region close to the pinhole) also being driven normal by current-induced pair breaking. This is far more difficult to quantify as we know little about the effective contact area for AR at the SC aluminium/N aluminium interface. Of course, both the Al pinhole and film are in a SC state purely due to the proximity effect with Nb, which further complicates quantitative analyses. However, in the bias range above 0.75 mV, we suppose that the AR occurs at a SC niobium/N aluminium (film) interface *again with its own conductance and enhancement*. It is, of course, important to remember that at any given bias there is only *one* N/SC interface at which AR may occur.

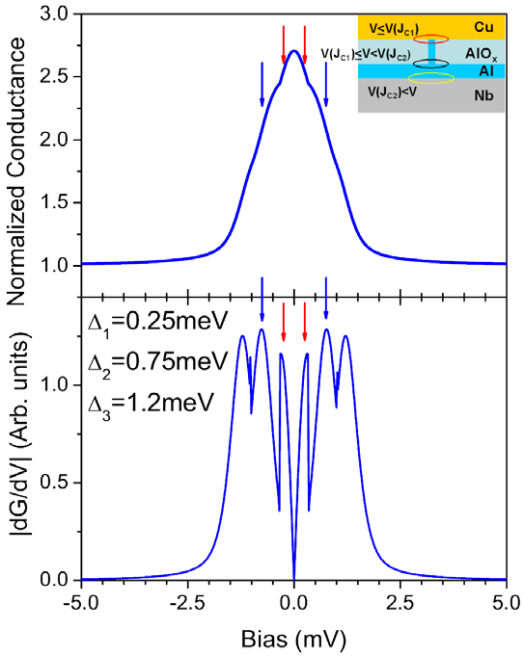

Figure 3. Calculated conductance and derivative spectra for a pinhole junction where AR takes place at one of three interfaces depending on the applied bias and current density. The interface at which AR occurs is shown schematically in the inset, which corresponds to a side-on view of the layer structure of the sample. Short (red) and long (blue) arrows indicate the parameters Δ_1 and Δ_2 respectively. This calculation is not a fit to the data in figure 2, but bears a qualitative resemblance.

We are now able to explain the 'extra' enhancement in the sub-gap conductance; in the ideal case there would be only an AR process at the SC aluminium pinhole/Cu electrode interface, producing an AR spectrum with a Δ parameter characteristic of aluminium and a factor of 2 conductance enhancement when normalized to the normal-state conductance of *that* interface. However, the experimental data are, in fact, normalized to the conductance of the *entire pinhole junction structure* in its normal state—thus the normalization is, in fact, to an entirely different contact. It is hardly surprising that the 'correct' conductance enhancement is not obtained. The important point to note here, in explaining the relevance to determining spin polarization accurately, is that for a magnetic electrode material the suppression of AR *will only occur for reflection processes occurring at the SC aluminium pinhole/FM electrode interface*; AR processes occurring at the other interfaces within the contact structure will significantly alter the value which would be extracted for the spin polarization.

Figure 3 shows the results of a simple model calculation for a single pinhole junction, based on the BTK formalism with $P = 0$ and $Z = 0$ for all interfaces and with $T = 2$ K. We assume that each contact has an identical nominal area and conductance for simplicity and offset the conductance curves by some amount G_{offset} so that the junction current is continuous across pair-breaking transitions which occur at bias $V(J_C)$, i.e. the junction current does not change discontinuously when either the pinhole or aluminium film are driven into the normal state. Summing the individual conductances in this fashion is equivalent to opening up additional ballistic conduction channels across the junction structure as the bias drops or, equivalently, as introducing additional resistance as the bias increases. The total 'normalized conductance' of

the pinhole junction as a function of (absolute) applied bias $G_{\mathrm{p}}(V)$ is thus given by

$$G_{\mathrm{p}}(V) = \begin{cases} G(\Delta_3, V) & \text{when} \quad V(J_{\mathrm{C}_2}) < V, \\ G(\Delta_2, V) + G_{\mathrm{offset}}(\Delta_3, V(J_{\mathrm{C}_2})) & \text{when} \quad V(J_{\mathrm{C}_1}) < V \leqslant V(J_{\mathrm{C}_2}), \\ G(\Delta_1, V) + G_{\mathrm{offset}}(\Delta_2, V(J_{\mathrm{C}_1})) & \text{when} \quad V \leqslant V(J_{\mathrm{C}_1}), \end{cases} \qquad \text{and}$$

where J_{C_i} and Δ_i are the critical current density and energy gap in layer i and each of the $G(\Delta, V)$ are derived from the BTK model. Representative energy gap values have been chosen for the three SC layers, depicted in the inset to figure 3, to clearly demonstrate the effect: Δ_1 represents the Al pinhole, Δ_2 the Al film and Δ_3 the Nb electrode. We point out that this calculation is in no way a fit to our data. For clarity, here we additionally specify the $V(J_{\mathrm{C}_i})$ so as not to be equal to any of the Δ_i in order to unambiguously distinguish features in the calculated PCAR and derivative spectra. The $V(J_{\mathrm{C}_i})$ may, in principle, be obtained from the *measured* junction conductance and the gap energies; this will in turn specify the G_{offset} through the current continuity condition, making the Δ_i the only 'fitting' parameters required.

This is, of course, a drastically simplified model which will certainly reproduce the features in the PCAR spectrum; what is somewhat more surprising is that it also reproduces the salient features in the derivative spectrum. The upper frame of figure 3 shows PCAR conductance, whilst the lower frame shows the absolute derivative spectrum; good correspondence with the experimental data from figure 2 is obtained even for such a simple model. The interesting point to note is that the peaks in the derivative spectrum clearly match the respective SC gap energies—this is far more difficult to determine from experimental data as the 'gap energy' is generally only obtained as a parameter from fitting to the PCAR data. Varying the Δ_i in the calculation results in the peak positions in the derivative spectrum shifting to the corresponding bias. The small spikes visible in the calculated derivative spectrum at ± 1 mV bias are an artefact of the current continuity condition and correspond to $V(J_{\mathrm{C}_2})$.

By comparing the two calculated spectra with our measurements, we are able to clearly associate features in both derivative *and* PCAR spectra with the SC gap energies of layers within the model contact structure. If we now return our attention to figure 2 we see that there are peaks in the derivative spectrum at energies of $\sim$0.4, $\sim$0.75 and $\sim$1.5 meV. The first and third of these correspond well to the accepted SC gap energies of aluminium and niobium respectively, while the other peak can be attributable to proximity effect induced superconductivity in the aluminium film. As noted earlier, the peaks at 0.4 and 0.75 meV allow us to explain the additional sub-gap conductance enhancement in the PCAR spectrum; we also note that the minimum in the conductance 'dip' occurs exactly at the energy of the derivative peak corresponding to the energy gap in niobium. This correspondence between experimental data and modelling allows us to clearly attribute this dip feature to a SC energy gap, as suggested from a modified-BTK-type calculation of Strijkers *et al* [5], and shows the inflections in the PCAR spectrum to be a signature of the critical current density effect.

4. Conclusion

To conclude, we have demonstrated a significantly larger enhancement in sub-gap conductance in a 50 nm diameter Nb/Al/Cu point contact junction in comparison to the expected conductance doubling due to Andreev reflection. We explain how this additional conductance enhancement may arise due to current-induced pair breaking within the layered pinhole junction, resulting in Andreev reflection taking place at different points within the structure depending on the level of applied bias. Further theoretical modelling beyond the simple BTK framework would be required in order to account for all of the features observed in these, and indeed many other, PCAR measurements. The observed conductance enhancement

demonstrates a potentially severe pitfall in the interpretation of spin-polarized point contact Andreev reflection data in nanoscale ferromagnet/superconductor point contacts; inflections in the PCAR spectra could prove to be a valuable diagnostic tool for determining critical current density effects in spin-polarized PCAR measurements.

Acknowledgments

The authors would like to thank G Burnell, V A Baltz, K P McKenna, L -A Michez and A Potenza for useful discussions; B T Donovan for assistance with micrometre PCAR measurements; and C S Allen, A D Naylor and A Walton for SEM imaging. We gratefully acknowledge financial support from EPSRC and from the EU via project NMP2-CT-2003-505587 'SFINx'.

References

[1] Andreev A F 1964 *Sov. Phys.—JETP* **19** 1228
[2] Soulen R J Jr, Byers J M, Osofsky M S, Nadgorny B, Ambrose T, Cheng S F, Broussard P R, Tanaka C T, Nowak J, Moodera J S, Barry A and Coey J M D 1998 *Science* **282** 85
[3] Upadhyay S K, Palanisami A, Louie R N and Buhrman R A 1998 *Phys. Rev. Lett.* **81** 3247
[4] Blonder G E, Tinkham M and Klapwijk T M 1982 *Phys. Rev.* B **15** 4515
[5] Strijkers G J, Ji Y, Yang F Y, Chien C L and Byers J M 2001 *Phys. Rev.* B **63** 104510
[6] Mazin I I, Golubov A A and Nadgorny B 2001 *J. Appl. Phys.* **89** 7576
[7] Xia K, Kelly P J, Bauer G E W and Turek I 2002 *Phys. Rev. Lett.* **89** 166603
[8] Perez-Willard F, Cuevas J C, Surgers C, Pfundstein P, Kopu J, Eschrig M and von Lohneysen H 2004 *Phys. Rev.* B **69** 140502
[9] Cespedes O, Clifford E and Coey J M D 2005 *J. Magn. Magn. Mater.* **290** 113
[10] Sharvin Y V 1965 *Sov. Phys.—JETP* **21** 655
[11] Miyoshi Y, Bugoslavsky Y and Cohen L F 2005 *Phys. Rev.* B **72** 012502
[12] Åkerman J J, Escudero R, Leighton C, Kim S, Rabson D A, Dave R W, Slaughter J M and Schuller I K 2002 *J. Magn. Magn. Mater.* **240** 86
[13] Hindmarch A T 2003 *PhD Thesis* University of Leeds
[14] Wolf E L 1985 *Principles of Electron Tunnelling Spectroscopy* (Oxford: Oxford University Press)
[15] Oliver B, Tuttle G, He Q, Tang X and Nowak J 2004 *J. Appl. Phys.* **95** 1315
[16] Romijn J, Klapwijk T M, Renne M J and Mooij J E 1982 *Phys. Rev.* B **26** 3648
[17] Sheet G, Mukhopadhyay S and Raychaudhuri P 2004 *Phys. Rev.* B **69** 134507